

A non-stationary space-time Gaussian Process model for partially converged simulations

Victor Picheny ^{*} David Ginsbourger [†]

Abstract

In the context of expensive numerical experiments, a promising solution to alleviate the computational costs consists of using partially converged simulations instead of exact solutions. The gain in computational time is at a price of precision in the response. This work addresses the issue of fitting a Gaussian process model to partially converged simulation data, for further use in prediction. The main challenge consists in the adequate approximation of the error due to partial convergence, which is correlated in both design variables and time directions. Here, we propose to fit a Gaussian process in the joint space of design parameters and computational time. The model is constructed by building a non-stationary covariance kernel that reflects accurately the actual structure of the error. Practical solutions are proposed to solve parameter estimation issues associated with the proposed model. The method is applied to a computational fluid dynamics test-case, and shows significant improvement in prediction compared to a classical kriging model.

keywords Kriging, computer experiments, covariance kernels

1 Introduction

Using computer experiments and metamodels for facilitating optimization and statistical analysis of engineering systems has become commonplace [Sacks et al. (1989); Jones et al. (1998); Santner et al. (2003)]. However, despite the continuous growth of computational capabilities, the complexity of simulators still drastically limit the number of available experiments, which are often insufficient to build accurate metamodels. An efficient solution to alleviate the computational cost consists in using degraded versions of the expensive simulator to provide faster but less accurate evaluations of the output. Such approximations can be obtained by using coarser mesh (in Finite Element methods), simpler partial differential equations, or geometry simplification for instance. The degraded simulator is often called low-fidelity (LF) model and the expensive version high-fidelity (HF) model.

Using metamodels in this context has been addressed by many authors in the literature. *Scaling* approaches [Lewis and Nash (2005)] approximate the difference between LF and HF models using a multiplicative or additive function. For instance, Alexandrov et al. (2000) and Gano et al. (2006) used polynomial response surfaces and kriging, respectively. Kennedy and O'Hagan (2000) proposed a so-called auto-regressive co-kriging model that allows integrating data with several fidelity levels into a single model. A generalization of this model is proposed in Qian and Wu (2008); its application for optimization can be found in Han et al. (2010), Huang et al. (2006), Forrester et al. (2007), Laurenceau and Sagaut (2008) or Yamazaki and Mavriplis (2011).

A less explored but promising alternative is to use partially converged simulations as a low-fidelity model, by artificially stopping solver convergence at early stage. Such approach has many advantages, among which the use of a single simulator instead of one simulator for each fidelity level, and the possibility of having as many levels of accuracy as desired. In Gumbert et al. (2001) and Dadone and Grossman (2000, 2003), partial

^{*}INRA, Toulouse, France (victor.picheny@toulouse.inra.fr)

[†]University of Bern, Switzerland (david.ginsbourger@stat.unibe.ch)

Table 1: Fixed points coordinates

	$P1$	$P2$	$P3$	$P4$	$P9$	$P10$	$P11$	$P12$
x	79.315	18.699	79.315	18.699	119.765	79.193	91.859	51.282
y	373.35	373.35	223.35	223.35	139.085	147.339	1.894	10.149

Table 2: Design variable bounds

	x_1	x_2	x_3	x_4	x_5	x_6	x_7
Lower bound	4	15	5	5	20	9	9
Upper bound	11	45	20	11	60	60	60

convergence is coupled with an adjoint formulation to solve fluid dynamic design problems at reasonable cost. Using metamodels with such data is an open and difficult question, that differs from the classical multifidelity framework since unconverged responses are likely to be a lot rougher than converged ones, and the number of fidelity levels can be very large. In the pioneer article of Forrester et al. (2006), it is observed that all simulations within the design space tend to converge in unison, so partially and fully converged responses are integrated in a co-kriging model as in a multifidelity framework. Although demonstrated to be quite efficient already, this approach somehow hinders the potential of partial convergence, since it allows the use of a very limited number of fidelity levels, and requires simulations to achieve a relatively high level of convergence. This work addresses the issue of fitting a metamodel to partially converged simulation data, when convergence levels potentially vary from one design to another. To do so, we propose to use a Gaussian process model in the joint space of design parameters and computational time. The model is based on a covariance kernel that accurately reflects the actual structure of the error.

In the next section, we describe a Computational Fluid Dynamics (CFD) simulation-based optimization problem, in which the calculated responses illustrates some important features of partially converged simulations. Then, we present a Gaussian process model indexed by the joint design-time space, followed by estimation issues and solutions specific to this model. Finally, the model is applied to the analysis of the CFD problem.

2 The S-shaped pipe flow model

To motivate our approach and highlight the important properties of partial convergence, we consider the optimization problem of an S-shaped pipe, whose form is defined parametrically. A two-dimensional CFD model is built using OpenFOAM and its solver *simpleFoam* (steady-state, incompressible, turbulent flow). A constant flow velocity is imposed at the pipe input, and a null pressure at the output. The pipe contour is defined with the help of eight fixed points (defined in Table 1) and seven parameters, as shown in Figure 1. The parameter bounds are given in Table 2. The objective is to maximize the uniformity of the flow velocity at the end of the S-section, so the objective function (referred to as f_{SD}) is taken as the velocity standard deviation between P9 and P10.

OpenFOAM allows us to monitor the velocity field for each solver step, so we can measure the convergence directly on the objective function. First, we generate 20 designs using Latin hypercube sampling (LHS), and for each solver step, we compute f_{SD} . Figure 2 shows the evolution of the 20 responses for all steps. Although converging to different values, all the convergence curves have similar shapes, and it seems reasonable to assume that most of the information required for prediction or optimization can be obtained before full convergence.

Now, in order to represent the data in the joint design-time space, we fix all the parameters to their nominal value but x_2 (which is the most sensitive parameter), and 100 designs are generated for x_2 values uniformly distributed between its bounds. For all designs, 500 solver iterations are used for convergence. Figure 3 shows three designs and their converged velocity fields, for minimum (left), mean (center) and maximum (right) values of x_2 .

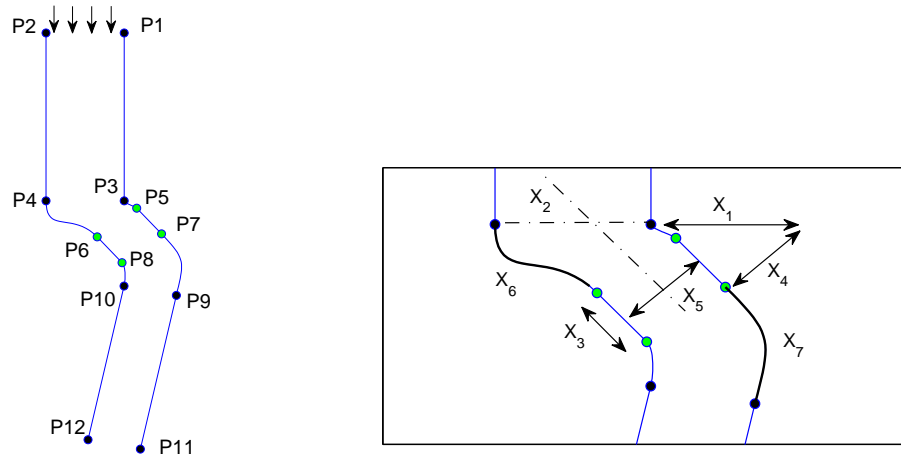


Figure 1: Contour and shape parameters of the 2D pipe model. x_2 is an angle, x_6 and x_7 define the curvatures of the Bezier curves (bold lines, right figure), x_1, x_3, x_4, x_5 are distances.

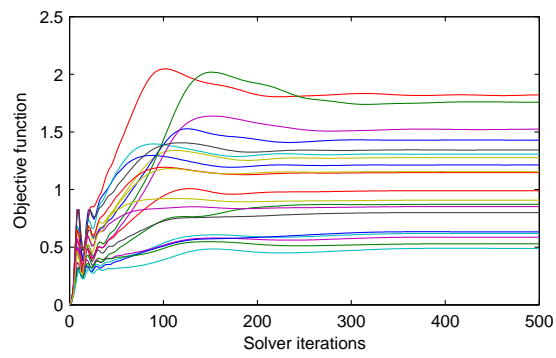


Figure 2: Response convergence for 20 designs.

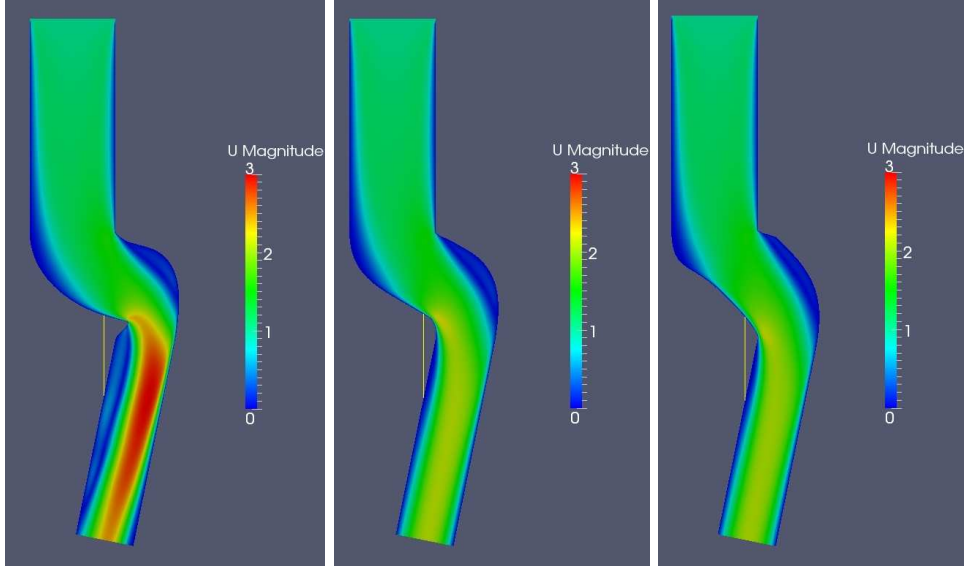


Figure 3: Three designs and velocity fields for x_2 taking its minimum (left), mean (center) and maximum values (right).

The objective function f_{SD} and the convergence error are then shown in the (x_2, t) plan (Figure 4), where t stands for the computation time (or number of iterations). The convergence error is here taken as the current objective function value minus the value at step 500.

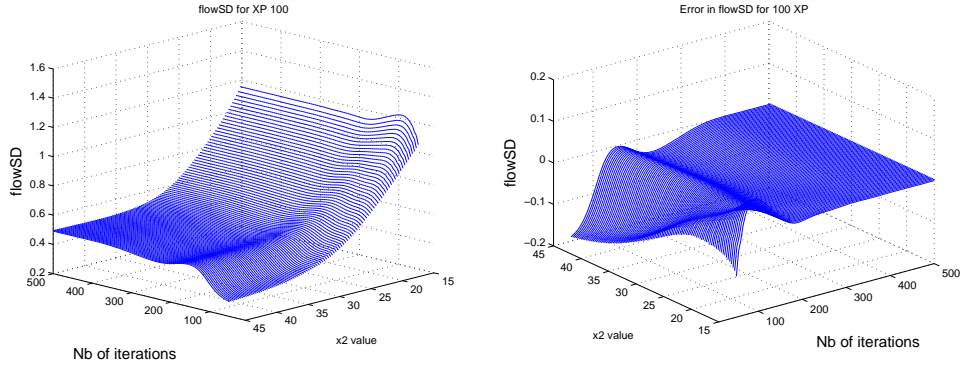


Figure 4: Evolution of objective function (left) and objective function error (right) as a function of x_2 and t . Time axis direction is reversed in the left figure to increase readability

First, we can observe that the response is smooth in both x_2 and t directions, which means that two close designs with the same number of convergence steps will have similar responses. Obviously, when t increases, the error decreases and tends towards zero, so the response becomes constant with respect to t . One can also observe that the error fluctuate with higher frequency for small t than for high t . These are the three key characteristics that we want to include in our model, as we describe in the next sections.

3 A brief review of the ordinary kriging (OK) model

This section contains a brief review of the ordinary kriging model, which is used as a basis for our space-time model.

3.1 OK equations

We denote by y the response of a numerical simulator or function that is to be studied: $y : \mathbf{x} \in D \subset \mathbb{R}^d \rightarrow y(\mathbf{x}) \in \mathbb{R}$. Taking the contemporary Bayesian interpretation [Rasmussen and Williams (2006)] of ordinary kriging [Matheron (1969)], y is assumed to be a realization of a Gaussian process (GP) Y with unknown constant mean μ and known covariance kernel k . In computer experiments, k is often assumed stationary (i.e. location-invariant). Kriging then amounts to conditioning the GP Y on a set of observed responses $\mathbf{Y} := y(\mathbf{X})$, where $\mathbf{X} = \{\mathbf{x}^i, 1 \leq i \leq n\}$ is a set of input parameters called the design of experiments. The conditional mean and variance of Y knowing \mathbf{Y} define respectively the kriging predictor m_{OK} and variance s_{OK}^2 , and are given by the following classical equations:

$$\begin{aligned} m_{OK}(\mathbf{x}) &= \mathbb{E}[Y(\mathbf{x}) | Y(\mathbf{x}^i) = y_i, 1 \leq i \leq n] \\ &= \hat{\mu} + \mathbf{k}(\mathbf{x})^T \mathbf{K}^{-1} (\mathbf{Y} - \hat{\mu} \mathbf{1}), \end{aligned} \quad (1)$$

and

$$\begin{aligned} s_{OK}^2(\mathbf{x}) &= \text{Var}[Y(\mathbf{x}) | Y(\mathbf{x}^i) = y_i, 1 \leq i \leq n] \\ &= k(\mathbf{x}, \mathbf{x}) - \mathbf{k}(\mathbf{x})^T \mathbf{K}^{-1} \mathbf{k}(\mathbf{x}) + \frac{(1 - \mathbf{1}^T \mathbf{K}^{-1} \mathbf{k}(\mathbf{x}))^2}{\mathbf{1}^T \mathbf{K}^{-1} \mathbf{1}} \end{aligned} \quad (2)$$

where:

- $|$ means “conditional on”,
- $\mathbf{Y} = (y(\mathbf{x}^1), \dots, y(\mathbf{x}^n))^T$,
- $\mathbf{K} = (k(\mathbf{x}^i, \mathbf{x}^j))_{1 \leq i, j \leq n}$,
- $\mathbf{k}(\mathbf{x}) = (k(\mathbf{x}, \mathbf{x}^1), \dots, k(\mathbf{x}, \mathbf{x}^n))^T$,
- $\mathbf{1}$ is a $n \times 1$ vector of ones, and
- $\hat{\mu} = (\mathbf{1}^T \mathbf{K}^{-1} \mathbf{Y})^{-1} (\mathbf{1}^T \mathbf{K}^{-1} \mathbf{1})$ is the best linear unbiased estimate of μ .

It is often assumed that the response is shifted by a polynomial trend instead of a constant; in universal kriging, a parametric trend is assumed and the corresponding trend coefficients are used in lieu of μ . This variant is not presented here for the sake of conciseness, but the proposed method applies without difficulty to it. Detailed calculations and statistical interpretation can be found in Cressie (1993) or Roustant et al. (2012) for instance.

When responses are observed in a Gaussian, independent noise, e.g. observations are of the form $Y(\mathbf{x}^i) + \varepsilon^i$ and $\text{cov}(\varepsilon^i, \varepsilon^j) = 0, i \neq j$, equations remain valid except that a diagonal matrix Δ has to be added to the covariance matrix \mathbf{K} at every occurrence [Rasmussen and Williams (2006), pp.16-17], with terms $\Delta_{i,j} = \text{cov}(\varepsilon^i, \varepsilon^j) = \delta_{i,j} \times \text{var}(\varepsilon^i), 1 \leq i, j \leq n$. Note that this model can be easily generalized to the case where the ε^i 's are correlated, Δ being then non-diagonal.

3.2 Covariance kernel and estimation of its parameters

In this work, the kernel used for spatial covariances in the design space is a stationary anisotropic kernel of the Matérn class, with smoothness parameter $\nu = 5/2$:

$$k(\mathbf{x}, \mathbf{x}') = \sigma^2 \left(1 + \sqrt{5} \|\mathbf{h}\|_{\Sigma} + \frac{5}{3} \|\mathbf{h}\|_{\Sigma} \right) \exp \left(-\sqrt{5} \|\mathbf{h}\|_{\Sigma} \right) \quad (3)$$

where $\mathbf{h} := \mathbf{x} - \mathbf{x}'$ and $\|\mathbf{h}\|_{\Sigma} := \sqrt{\mathbf{x}^T \Sigma \mathbf{x}'}$, with $\Sigma = \text{diag}([1/\theta_1^2, \dots, 1/\theta_d^2])$. The matrix Σ accounts for anisotropy in the \mathbf{x} space.

The parameters σ^2 and $\theta_1, \dots, \theta_d$ are often referred to as *process variance* and *ranges*, respectively. They are usually not known in advance by the user and must be estimated based on a sample of observations. One of the most popular method to do so is the maximum likelihood estimation (MLE), which amounts to maximizing the probability density function at \mathbf{Y} of the observations $Y(\mathbf{X})$, seen as a function of the covariance parameters:

$$\left\{ \hat{\sigma}^2, \hat{\theta}_1, \dots, \hat{\theta}_d \right\} \in \arg \min (2\pi)^{-\frac{n}{2}} \det(\mathbf{K})^{-\frac{1}{2}} \exp \left(-\frac{1}{2} (\mathbf{Y} - \hat{\mu}\mathbf{1})^T \mathbf{K}^{-1} (\mathbf{Y} - \hat{\mu}\mathbf{1}) \right) \quad (4)$$

In the case of noiseless observations, \mathbf{K} can be factorized by σ^2 : $\mathbf{K} = \sigma^2 \mathbf{R}$ (with \mathbf{R} not depending on σ^2). Then, for fixed $\theta_1, \dots, \theta_d$, the optimal σ^2 is given by:

$$\hat{\sigma}^2 = \frac{1}{n} (\mathbf{Y} - \hat{\mu}\mathbf{1})^T \mathbf{R}^{-1} (\mathbf{Y} - \hat{\mu}\mathbf{1}) \quad (5)$$

By injecting this quantity into equation 4 and applying a logarithmic transformation, the MLE problem simplifies to the minimization of the so-called *concentrated (or "profile") log-likelihood* with respect to the range parameters only:

$$\left\{ \hat{\theta}_1, \dots, \hat{\theta}_d \right\} = \arg \min n \log \left(\frac{1}{n} (\mathbf{Y} - \hat{\mu}\mathbf{1})^T \mathbf{R}^{-1} (\mathbf{Y} - \hat{\mu}\mathbf{1}) \right) + \log(\det(\mathbf{R})), \quad (6)$$

the MLE of σ^2 being computed afterwards using equation 5. The reader can refer to Stein (1999) (chapter 6) or Rasmussen and Williams (2006) (chapter 5) for additional details.

4 A Gaussian process surrogate for partially converged simulations

The OK model presented in the previous section relies on a set of assumptions, in particular the stationarity of the response Y , that are approximately met in many computer experiments situations. Here, the particular behavior of the response strongly violates some of these assumptions. This section presents a model based, like OK, on Gaussian process conditioning, that fits adequately partially converged responses.

4.1 Desired properties

When partial convergence is considered, an observation y_i is defined by both input parameters $\mathbf{x} \in D$ and computational time $t \in (0, +\infty)$ (typically equal or proportional to the number of solver iterations). Now, for a fixed \mathbf{x} , the response evolves in a very specific non-stationary way as a function of t , in the flavour of a damped signal with decreasing oscillation frequency. As will be illustrated here, Gaussian processes are particularly well suited to predict such types of responses, since they allow defining models that can inherit such kind of assumed structure on the function to approximate.

The problem of joint space-time modeling has been addressed by many authors, see Kyriakidis and Journal (1999) for a review. However, the specific behavior of the responses observed here requires to design an *ad hoc* model.

We consider here that the observed function is a realization of a GP $Y(\mathbf{x}, t)$, sum of a GP F indexed by \mathbf{x} only, and a GP G indexed by \mathbf{x} and t :

$$Y(\mathbf{x}, t) = F(\mathbf{x}) + G(\mathbf{x}, t), \quad (7)$$

where F stands for the response under complete convergence and G is an error term due to partial convergence. In addition, we assume that F and G are independent.

Although not based on physical considerations, such assumptions were found to be reasonable (See §7) and have many advantages, since observations are decomposed between what we are interested in (the actual response) and what we want to filter out (the error term).

The actual response F may be modeled under the usual assumptions made in kriging for computer experiments [Sacks et al. (1989)], such as stationarity. The error G , however, has a more specific structure. Under the hypothesis of independence between F and G , the kernel k_Y of Y simply writes as the sum of the kernels of F and G , so all the modeling difficulty lies in the characterization of the convergence error G .

In the \mathbf{x} space, it can be observed (Figure 4) that two runs with close sets of input parameters converge in a similar fashion, hence their convergence errors are correlated. In the t direction, except for the first few iterations that often show large oscillations, the convergence is smooth so the responses evaluated at successive steps are also correlated. In addition, the convergence error tends to zero when the computational time increases. It is reasonable to assume that the error variance decreases monotonically with computational time, which makes G non-stationary in the t direction. The speed of convergence may differ slightly from one design to another, but assuming this speed to be constant seems reasonable here. Finally, one can observe that the oscillation frequency of the error tends to decrease with time, which is another non-stationary behavior in the t direction.

4.2 Modifying usual covariance functions

Most usual covariance functions in the kriging framework are stationary (i.e. $k(\mathbf{x}, \mathbf{x}')$ is a function of $\mathbf{x} - \mathbf{x}'$), hence are not suitable for our problem. However, lots of possibilities exist to modify usual kernels to make new ones with the desirable properties, see Rasmussen and Williams (2006) (chapter 4, pp.94-95) for a detailed discussion. In particular, we use here the three following properties:

- given two positive definite kernels (a characterization of positive-definiteness is given below) $k_1(\mathbf{x}, \mathbf{x}')$ and $k_2(\mathbf{x}, \mathbf{x}')$, their sum k_3 and product k_4 are positive definite kernels:

$$k_3(\mathbf{x}, \mathbf{x}') = k_1(\mathbf{x}, \mathbf{x}') + k_2(\mathbf{x}, \mathbf{x}'), \quad k_4(\mathbf{x}, \mathbf{x}') = k_1(\mathbf{x}, \mathbf{x}') \times k_2(\mathbf{x}, \mathbf{x}')$$

- given any function $a : D \rightarrow D$, the following kernel is positive definite:

$$k_5(\mathbf{x}, \mathbf{x}') = k(a(\mathbf{x}), a(\mathbf{x}'))$$

Proofs are direct by verifying that the following characterization is met:

A kernel k on $D \times D$ is positive definite if and only if it is symmetric ($k(\mathbf{x}, \mathbf{x}') = k(\mathbf{x}', \mathbf{x})$ for all $\mathbf{x}, \mathbf{x}' \in D$) and for all $\{\mathbf{x}_1, \dots, \mathbf{x}_n\} \in D$ ($n \in \mathbb{N}$) and all $\{a_1, \dots, a_n\} \in \mathbb{R}$:

$$\sum_{i,j=1}^n a_i a_j k(\mathbf{x}_i, \mathbf{x}_j) \geq 0 \quad (8)$$

4.3 A covariance kernel for partial convergence

Recall that G is a process indexed by \mathbf{x} and t , with decreasing amplitude and oscillation frequency when t increases. To account for the decreasing amplitude, we propose to use a covariance of the form:

$$k_G(\mathbf{u}, \mathbf{u}') = \sigma(t)\sigma(t')r_G(\mathbf{x}, \mathbf{x}', t, t') \quad (9)$$

where $\mathbf{u} = (\mathbf{x}, t)$, r_G is a correlation kernel and $\sigma(t)$ is a decreasing function of t . Since G tends to zero, $\sigma(t)$ should be null when $t \rightarrow +\infty$. Here we choose a decreasing exponential:

$$\sigma(t) = \sigma_G^2 \exp(-\alpha t), \quad (10)$$

with $\alpha \in (0, +\infty)$ a parameter that accounts for the convergence speed. Note that the case of non-null asymptotic error (due to discretization, inaccurate application of boundary conditions or limit cycles in the convergence, see Forrester et al. (2006)) can be treated easily by setting the limit to a positive constant instead of zero.

Although not necessary, it is convenient to choose a separable function for r_G :

$$r_G(\mathbf{u}, \mathbf{u}') = r_{Gx}(\mathbf{x}, \mathbf{x}') \times r_{Gt}(t, t'), \quad (11)$$

which allows to handle different regularities in \mathbf{x} and t directions. The correlation r_{Gx} can be taken as stationary, for instance, the Matérn kernel of equation 3.

The correlation r_{Gt} has to account for the increasing smoothness of the error (high oscillations for the first steps, then smoother convergence). To do so, we propose to use a classical covariance (for instance the Matern 5/2 function) and plug in a non-linear change of variables in it so as to obtain the desirable effect, e.g. using a transformation of the form:

$$a(t) = \frac{1}{\zeta + \eta t}, \quad (12)$$

where $\zeta, \eta \in (0, +\infty)$, leading to a covariance kernel depending on the increment

$$a(t) - a(t') = \frac{t' - t}{\frac{\zeta^2}{\eta} + \zeta(t + t') + \eta t t'} \quad (13)$$

The properties stated in the previous section ensure that k_G is a positive definite kernel.

Finally, by independence, Y 's kernel is the sum of F 's and G 's kernels:

$$k_Y(\mathbf{u}, \mathbf{u}') = k_F(\mathbf{x}, \mathbf{x}') + k_G(\mathbf{u}, \mathbf{u}'), \quad (14)$$

where k_F is a standard covariance (e.g. Matérn 5/2). Using this kernel, we are able to perform simulation, conditional simulation, hence learning with Gaussian processes.

Let $\mathbf{Y}_n = [y_1, \dots, y_n]^T$ be a set of observations, \mathbf{X} the matrix of design parameters, \mathbf{T} the vector of times and $\mathbf{U} = [\mathbf{X}, \mathbf{T}]$ the experimental matrix. In the fashion of OK, the mean and variance of Y at $\mathbf{u}^* = (\mathbf{x}^*, t^*)$ conditional on the observations \mathbf{Y} are given by:

$$m(\mathbf{u}^*) = \hat{\mu} + \mathbf{k}_Y(\mathbf{u}^*)^T \mathbf{K}_Y^{-1} (\mathbf{Y} - \hat{\mu} \mathbf{1}) \quad (15)$$

$$s^2(\mathbf{u}^*) = k_Y(\mathbf{u}^*, \mathbf{u}^*) - \mathbf{k}_Y(\mathbf{u}^*)^T \mathbf{K}_Y^{-1} \mathbf{k}_Y(\mathbf{u}^*) + \frac{(1 - \mathbf{1}^T \mathbf{K}_Y^{-1} \mathbf{k}_Y(\mathbf{x}))^2}{\mathbf{1}^T \mathbf{K}_Y^{-1} \mathbf{1}} \quad (16)$$

with: $\mathbf{K}_{Yi,j} = k_Y(\mathbf{u}^i, \mathbf{u}^j)$, $\mathbf{k}_Y = [k_Y(\mathbf{u}^*, \mathbf{u}^1) \dots k_Y(\mathbf{u}^*, \mathbf{u}^n)]$ and $\hat{\mu} = \frac{\mathbf{1}^T \mathbf{K}_Y^{-1} \mathbf{Y}}{\mathbf{1}^T \mathbf{K}_Y^{-1} \mathbf{1}}$.

The functions $m(\cdot)$ and $s^2(\cdot)$ define the Gaussian process model, which provides a prediction and a prediction variance for any design with given convergence level. As for the standard OK model, m is equal to the observations and s is equal to zero at any \mathbf{u}^i ($1 \leq i \leq n$).

In most applications, in particular for optimization, the value of interest is the actual response, i.e. the asymptotic value for $t \rightarrow \infty$. From equation 14, the covariance $k_Y(\mathbf{u}, \mathbf{u}^*)$ is defined for $\mathbf{u}^* = (\mathbf{x}^*, \infty)$ and is simply equal to $k_F(\mathbf{x}, \mathbf{x}^*)$ (indeed, $\lim_{t \rightarrow \infty} \sigma_G(t) = 0$ which implies $k_G = 0$). Then, we can define an asymptotic prediction independent of t , equal to:

$$m_\infty(\mathbf{x}^*) = \hat{\mu} + \mathbf{k}_F(\mathbf{x}^*)^T \mathbf{K}_Y^{-1} (\mathbf{Y} - \hat{\mu} \mathbf{1}) \quad (17)$$

$$s_\infty^2(\mathbf{x}^*) = \sigma_F^2 - \mathbf{k}_F(\mathbf{x}^*)^T \mathbf{K}_Y^{-1} \mathbf{k}_F(\mathbf{x}^*) + \frac{(1 - \mathbf{1}^T \mathbf{K}_Y^{-1} \mathbf{k}_F(\mathbf{x}))^2}{\mathbf{1}^T \mathbf{K}_Y^{-1} \mathbf{1}} \quad (18)$$

One can notice that these equations take the form of an ordinary kriging with correlated residuals, since $\mathbf{K}_Y = \mathbf{K}_F + \mathbf{K}_G$, \mathbf{K}_G playing the role of Δ in §3.

4.4 Discussion

4.4.1 Comparison with co-kriging

One might prefer to limit the responses to two (or a few) convergence levels only, as in [Forrester et al. (2006)]. In that case, the data is similar in form to a multi-fidelity framework, for which the co-kriging model [Kennedy and O'Hagan (2000); Qian and Wu (2008)] has been proved to be an efficient tool for prediction and optimization.

When t levels of response are considered, the co-kriging model assumes that the more accurate response Z_t is equal to the less accurate response Z_{t-1} multiplied by a scaling factor ρ_{t-1} plus a stationary Gaussian process independent of Z_t and Z_{t-1} :

$$Z_t(\mathbf{x}) = \rho_{t-1}Z_{t-1}(\mathbf{x}) + \delta_t(\mathbf{x}) \quad (19)$$

In the framework of this paper, we have $Z_t(\mathbf{x}) = F(\mathbf{x}) + G(\mathbf{x}, t)$ and $Z_{t-1}(\mathbf{x}) = F(\mathbf{x}) + G(\mathbf{x}, t-1)$. Hence, the two models differ for two reasons. First, by the scaling factor ρ_t : this factor is intuitive in a multi-fidelity framework, since data may come from different simulators, so they are different in nature and may have different amplitudes. This behavior is not so clear with partial convergence.

The second difference is the co-kriging assumption of independence of the differences between two fidelity levels: $cov(\delta_{t_1}(\mathbf{x}), \delta_{t_2}(\mathbf{x})) = 0, t_1 \neq t_2$. This would imply that $G(\mathbf{x}, t_1)$ is independent of $G(\mathbf{x}, t_2)$, which is obviously false from Figure 2. Co-kriging might apply to partial convergence only if the convergence times t_1, t_2, \dots are sparse enough so the hypothesis of independence of the differences holds.

4.4.2 Monte-Carlo convergence

The space-time model allows us to deal with a framework closely related to partial convergence that is typical of robust design for instance: an observation is computed by averaging an arbitrary number t_i of independent drawings (or repeated experiments):

$$\tilde{Y}_i = \frac{1}{t_i} \sum_{j=1}^{t_i} F(\mathbf{x}_i) + \varepsilon_{i,j}, \quad (20)$$

when $F(\mathbf{x})$ is the function of interest, observed with noise $\varepsilon_{i,j} \sim \mathcal{N}(0, \tau^2)$. We have then $\tilde{Y}_i \sim \mathcal{N}\left(F(\mathbf{x}_i), \frac{\tau^2}{t_i}\right)$. F is observed exactly for $n_i \rightarrow +\infty$, and the process error G is equal to:

$$G(\mathbf{x}^i, t^i) = \frac{1}{t_i} \sum_{j=1}^{t_i} \varepsilon_{i,j}, \quad t_i \leq n_i \quad (21)$$

In a classical framework, one would only use the observation \tilde{Y}_i and build a kriging with noisy observations by adding diagonal terms $\frac{\tau^2}{n_i}$ to the covariance matrix, as explained in §3. In contrast, the space-time model presented here takes the whole trajectory of G into account, that is $\{G(\mathbf{x}^i, 1), \dots, G(\mathbf{x}^i, t_i)\}$. One may wonder if this adds any helpful information for prediction. We show below that the two models are actually equivalent, due to the Markovian property of G here.

Indeed, since all $\varepsilon_{i,j}$ are uncorrelated, the covariance of G is null in the x direction:

$$cov(G(\mathbf{x}^i, t^i), G(\mathbf{x}^j, t^j)) = 0 \text{ for any } \mathbf{x}^i \neq \mathbf{x}^j$$

For a given trajectory (fixed $\mathbf{x}^i, t_i^{(1)}, t_i^{(2)} \leq t_i$), it is easy to find that we have:

$$cov\left(G(\mathbf{x}^i, t_i^{(1)}), G(\mathbf{x}^i, t_i^{(2)})\right) = \frac{\tau^2}{\max(t_i^{(1)}, t_i^{(2)})} = \tau^2 \frac{\min(t_i^{(1)}, t_i^{(2)})}{t_i^{(1)} t_i^{(2)}} \quad (22)$$

So the kernel of G is:

$$k_G((\mathbf{u}^i, t_i^p), (\mathbf{u}^j, t_j^q)) = \frac{\tau^2}{t_i^{(p)} t_j^{(q)}} \min(t_i^{(p)}, t_j^{(q)}) \delta_{\mathbf{x}^i = \mathbf{x}^j} \quad (23)$$

where $\mathbf{u}^i = \{\mathbf{x}^i, t_i^{(p)}\}$ and $\mathbf{u}^j = \{\mathbf{x}^j, t_j^{(q)}\}$, $1 \leq t_i^{(p)} \leq t_i$, $1 \leq t_j^{(q)} \leq t_j$.

With such kernel, we show that given a (space-time) model conditioned on the observations \tilde{Y}_i (as defined in 20), adding any $Y(u)$ with $u = (\mathbf{x}^i, t_u)$ for $i \in \{1, \dots, n\}$ and $t_u \leq t_i$ has no effect on the model. This property can be seen as a *screening effect* [Stein (2002)] in the time dimension. The proof is given in the appendix. Note that this effect is true only when the covariance is Markovian in the time direction and null in the \mathbf{x} direction.

Hence, in this case the space-time model coincides with a kriging with noisy observations, so taking into account the convergence trajectories is useless. The use of space-time models makes sense only when the convergence path is not Markovian or when the errors are correlated in the \mathbf{x} direction.

4.5 Generalization and limitations

The model presented in this section assumes that all simulations within the design space converge similarly, that is, convergence errors may take different values but their amplitude, at a given computational time, is approximately the same. Hence, the model does not take into account the case where convergence behaviour varies significantly between two designs, for instance when limit cycles are observed for a fraction of the design space. In theory, the model can be generalized easily to such cases by modifying appropriately the covariance of G , for instance by choosing a function $\sigma(t)$ dependent on \mathbf{x} . However, it may come at a price of additional parameters that might make the learning stage overly challenging.

Secondly, the usefulness of this model depends on the shape of the convergence error. For simulators that require many steps to achieve a reasonable error (in contrast, only 50 are required in Figure 2), e.g. boundary layer and shock dominated flows, and / or converge very quickly once in the asymptotic convergence regime as exhibited in full Newton solvers, the computational savings of partial convergence may be either not realizable or somewhat limited. In any case, it can be noted that the convergence error behaviour not only depends on the solver but also on the objective function considered. In the problem described in §2, the objective function is the standard deviation of the flow velocity over a section: its associated error may be a lot smoother than for an objective function based, say, on the velocity at a single point. Hence, in the application considered in this article, the method provide substantial improvement (as shown in §7), but a different function might lead to different performances.

5 Estimating model parameters

In ordinary kriging, the covariance parameters are most of the time estimated by optimizing a criterion of fit, for instance by maximizing the likelihood of the parameters given the observations, or by minimizing the cross-validation error. This step is particularly critical for the accuracy of the kriging model, and is known to be difficult, in particular when the number of observations is small and the number of parameters large. Our model requires the knowledge of the parameters of k_Y . Assuming anisotropy in the \mathbf{x} space and the Matérn 5/2 class for all underlying kernels, we have:

- for the stationary covariance k_F : $d + 1$ parameters, $\sigma_F^2, \theta_F^1, \dots, \theta_F^d$,
- for the stationary correlation r_{Gx} : d parameters, $\theta_G^1, \dots, \theta_G^d$,
- for the correlation r_{Gt} : two parameters, η and ζ ,
- for the process variance σ^2 : two parameters, σ_G^2 and α .

Learning these $2d + 5$ parameters in a single optimization loop seems unrealistic here, since the objective function is likely to be highly multi-modal, and ensuring a good exploration may be too expensive computationally.

Besides, with partial convergence, the design of experiments takes a particular form, which can be used to simplify the estimation procedure. Indeed, when an observation is made at \mathbf{x} with time t , the response can be calculated without any computational effort for all the steps smaller than t . In other words, one has access

to the response convergence for the design \mathbf{x} from one to t : $\{y(\mathbf{x}, 1), y(\mathbf{x}, 2), \dots, y(\mathbf{x}, t)\}$. In the following, we refer to a series of data for the same \mathbf{x} and increasing t as *response* (or *error*) *trajectory*. Then, we propose to decompose the kernel parameter estimation into two steps: first, we estimate the parameters related to time only, and then the parameters related to \mathbf{x} .

5.1 Estimating t-space parameters

$\sigma(t)$ accounts for the convergence speed of the simulator (the variance of the error due to partial convergence). This speed might differ from one design to another, especially if the design space is large, but it is reasonable to consider speed as uniform, and then estimate it from a small number of simulations.

We assume here that the user has performed a small number K of fully converged simulations ($3 \leq K \leq 10$, typically), well spread in the design space. Let N be the number of steps required for full convergence, we have then an initial set of $K \times N$ observations:

$$\{y(\mathbf{x}_1, t_1), \dots, y(\mathbf{x}_1, t_N), \dots, y(\mathbf{x}_K, t_1), \dots, y(\mathbf{x}_K, t_N)\}.$$

The error trajectories can be known exactly by subtracting the converged responses to the partially converged response trajectories: $g(\mathbf{x}_i, t_j) = y(\mathbf{x}_i, t_j) - y(\mathbf{x}_i, t_N)$. We have then realizations of the process G for K designs and N times:

$$g(\mathbf{x}_1, t_1), \dots, g(\mathbf{x}_1, t_N), \dots, g(\mathbf{x}_K, t_1), \dots, g(\mathbf{x}_K, t_N).$$

We assume then that the correlation in \mathbf{x} is null, which is reasonable considering that K is very small and the observations are away one from each other. In that case, we have:

$$k_G((\mathbf{u}^i, \mathbf{u}^j)) = \sigma(t_i)\sigma(t_j)r_{Gt}(t_i, t_j)\delta_{\mathbf{x}^i=\mathbf{x}^j} \quad (24)$$

The parameters σ_G^2 , η , ζ and α can then be estimated by MLE, i.e. by solving:

$$\min_{\{\sigma_G^2, \eta, \zeta, \alpha\}} l = \log \det \mathbf{K}_G + \mathbf{g}^T \mathbf{K}_G^{-1} \mathbf{g} \quad (25)$$

As for ordinary kriging, the covariance matrix can be factorized by σ_G^2 : $\mathbf{K}_G = \sigma_G^2 \mathbf{R}_G$, so the concentrated log-likelihood can be used:

$$\{\hat{\eta}, \hat{\zeta}, \hat{\alpha}\} = \arg \min \left[KN \log \left(\frac{1}{KN} \mathbf{g}^T \mathbf{R}_G^{-1} \mathbf{g} \right) + \log (\det (\mathbf{R}_G)) \right] \quad (26)$$

$$\hat{\sigma}_G^2 = \frac{1}{KN} \mathbf{g}^T \mathbf{R}_G^{-1} \mathbf{g} \quad (27)$$

This problem is only three-dimensional, which makes it easy to solve. Moreover, computing the concentrated log-likelihood is here facilitated since \mathbf{R}_G is block-diagonal (see §6).

5.2 Estimating x-space parameters

Once the time-related parameters are estimated, the remaining unknown parameters are related to the covariance of F (σ_F^2 , $\theta_F^1, \dots, \theta_F^d$) and the correlation r_x of G ($\theta_G^1, \dots, \theta_G^d$). The direct optimization of the log-likelihood may be overly challenging, especially if d is large. In order to reduce the problem dimension, we assume that F and G share the same anisotropy, i.e. the respective influence of the parameters will be the same for the actual process and the error. Thus, we set:

$$\theta_G^i = \rho \theta_F^i, \quad 1 \leq i \leq d \quad (28)$$

with ρ a factor of proportionality.

The number of parameters is then reduced to $d + 2$, which makes it feasible to use MLE, hence solving the problem:

$$\{\hat{\sigma}_F^2, \hat{\theta}_F^1, \dots, \hat{\theta}_F^d, \hat{\rho}\} = \arg \min \left(\log \det \mathbf{K}_Y + (\mathbf{Y} - \hat{\mu}\mathbf{1})^T \mathbf{K}_Y^{-1} (\mathbf{Y} - \hat{\mu}\mathbf{1}) \right) \quad (29)$$

Note that here, the matrix \mathbf{K}_Y cannot be factorized by σ_F^2 , so concentrated log-likelihood cannot be used to estimate σ_F^2 separately.

6 Numerical issues

The major numerical issue with partial convergence comes from the huge amount of data available. The covariances matrices used either for parameter learning or prediction are of very large size, and their inversion can be at the same time computationally intensive and subject to numerical instabilities.

A first numerical trick to facilitate the inversion, well-known to kriging users, consists of adding a small diagonal matrix (nugget) to the covariance matrix, which amounts to relaxing the constraint of exactly interpolating the data. Here, since the diagonal of \mathbf{K}_G is not constant and typically shows variations of several orders of magnitude, it is preferable to add a value proportional to the diagonal term, for instance $10^{-4} \times \sigma(t_i)\sigma(t_i)$. Thus, the relaxation is similar for all the data points.

Another natural option to reduce the computational cost is to use only a subset of the available data. This solution is discussed separately for the parameter learning and prediction situations.

6.1 Data reduction for parameter estimation

The first step of parameter estimation is to use a small number K of error trajectories to estimate the time-related parameters. Since the trajectories are assumed to be independent of each other, the matrix \mathbf{K}_G is block diagonal: $\mathbf{K}_G = \text{diag}(\mathbf{K}_G^1, \dots, \mathbf{K}_G^K)$. Then, we have:

$$\begin{aligned} \log(\det(\mathbf{K}_G)) &= \prod_{k=1}^K \log(\det(\mathbf{K}_G^k)) \\ \mathbf{K}_G^{-1} &= \text{diag}((\mathbf{K}_G^1)^{-1}, \dots, (\mathbf{K}_G^K)^{-1}) \end{aligned}$$

The matrices \mathbf{K}_G^i are of size $N \times N$ (N being the number of steps required to achieve full convergence). N typically varies from hundreds (as for the application presented here) to thousands for complex simulations. If it is too large, one must use a subset of the data only. Regular subsets (one observation every p steps) may ensure a better inference of the error decrease rate (parameters α and σ_G), but this is at the price of the regularity information (local smoothness), which may impact the estimation of η and ζ . Irregular sub-sampling may offer the best trade-off.

When estimating the parameters related to the \mathbf{x} space, using a subset of the data seems particularly necessary since the inversion of \mathbf{K}_Y is embedded in an optimization loop and is likely to be calculated numerous times. The question is then how to choose the subset that will provide the most information about k_G and k_F . Choosing the last point of each trajectory seems obvious since these points provide the most information on F . In addition, the subset should favor data with equal times (i.e. alignments in the t direction), since they are the points with highest correlation value across trajectories.

6.2 Data reduction for prediction

It is well-known that for most kernels, the classical kriging predictor at a location \mathbf{x}^* is mainly determined by the few observations nearest to the prediction point, so that a kriging based only on these neighbor observations provides nearly the same predictor (and prediction variance) than the kriging with all the observations. This phenomenon is often called *screening effect* [Cressie (1993); Stein (2002)], and is used to compute fast predictions in the case of large data sets. Data selection is typically performed by building a hyper-rectangle (or ellipsoid) in the \mathbf{x} space, centered on the prediction point.

The definition of neighborhood in our context is not straightforward for the asymptotic prediction, i.e. prediction of the actual response F . Indeed, with the convention $t = \infty$ for asymptotic prediction, all the observations are equally far away (in terms of Euclidean distance) from the prediction point in the time space.

A simple conservative approach consists of selecting all the data for which $k_F(\mathbf{x}^*, \mathbf{x}^i)$ is higher than a certain level, or equivalently, define the neighborhood of \mathbf{x}^* as:

$$\Omega = \{\mathbf{x} \in D \mid \frac{1}{\sigma_F^2} k_F(\mathbf{x}^i, \mathbf{x}^*) > \beta\} \quad (30)$$

for some level $0 \leq \beta \leq 1$. This ensures (see equations 15 and 16) that all the influent observations are taken into account, but may select a lot more observations than actually necessary.

Indeed, as we noticed before, the last term of a trajectory (corresponding to the highest computational time) is the one that contains the most information for asymptotic prediction. However, since the trajectories are not Markovian, the other terms also have an influence on the prediction. In particular, the very last terms provide (seeing it as finite differences) the derivative information of G in the t direction.

Hence, we propose as a rule of thumb to choose the last three observations of each trajectory in Ω as our subset for asymptotic prediction.

7 Application to the pipe flow example

In this section, we illustrate the learning steps of the previous section applied to the data of the CFD example. For this analysis, two data sets are generated, one for learning and the other for testing. Both are based on 200-point LHS designs with *maximin* criterion. Some combination of parameters lead to unfeasible configurations (detected at the meshing stage) and are removed from the data sets (14 points for the learning set and 18 for the test set).

7.1 Estimating t-space parameters

Four points, randomly chosen in the first LHS, are used to generate fully converged runs (with 500 steps), from which we extract the corresponding error trajectories. For each trajectory, the first 50 steps are removed since the convergence behavior is non-smooth. By construction (see §5.1), the last term of each error trajectory is zero, which is slightly incorrect (the actual error is of the order of the solver tolerance). To avoid bias, the last 20 steps are also removed. The corresponding data (1720 error values) is represented in Figure 6 (left).

Then, the likelihood function of the full dataset is optimized using a $32 \times 32 \times 32$ grid (with realistic bounds for the parameters). We found $\hat{\sigma}_G^2 = 0.247$, $\hat{\alpha} = 0.0128$, $\hat{\eta} = 66.5$ and $\hat{\zeta} = 1/60$. Figure 5 shows the concentrated likelihood in the α - η direction at optimal ζ ; the optimization problem is here unimodal and the optimal values are well-defined.

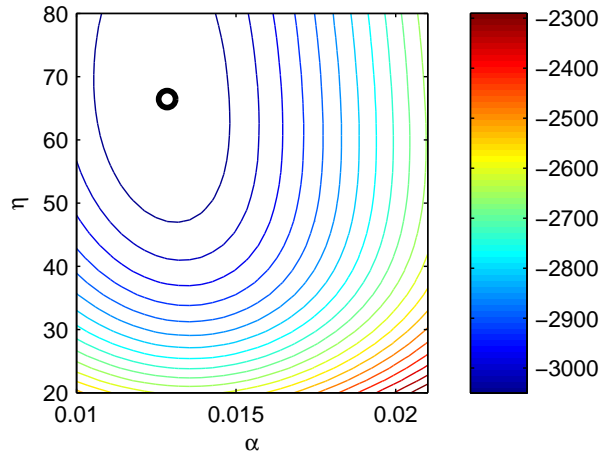


Figure 5: Concentrated likelihood contour lines in the α - η space at optimal ζ .

To validate visually that the error model is well calibrated (i.e. $\hat{\sigma}_G^2$ and $\hat{\alpha}$ are realistic), we draw in Figure 6 (right) the error trajectories divided by $\sigma(t)^2$. If the values are well-chosen, the normalized trajectories must be stationary with variance equal to one. Here, this seems (approximately) true. One can notice that the amplitude of the curves are non-constant, which indicates that the model might be improved by

considering a process variance that also depends on \mathbf{x} . However, this would make the learning problem very difficult to solve.

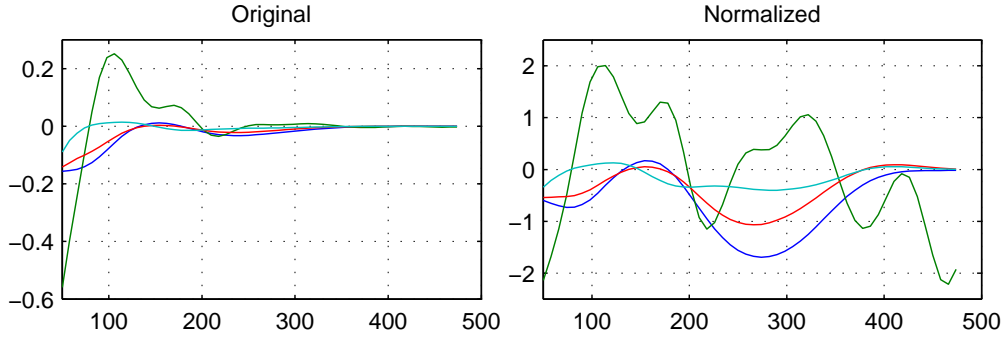


Figure 6: Original error trajectories and rescaled trajectories using estimated parameters.

In order to illustrate the error model, we represent the actual error trajectory of a new design (randomly chosen), and the associated Gaussian process model based on 20 observations of this trajectory, uniformly chosen between $t = 0$ and $t = 500$. The trajectory and GP model (mean and 95% confidence interval) are shown in Figure 7. Note that such kind of data is not realistic, since in a real case the response would be known for all the intermediate steps, but the shape of the GP mean and confidence interval reflects the accuracy of the model. Here, the smoothness of the model mean is similar to the one of the actual process, except for the very first steps, where it shows very high variability. The confidence intervals are also quite realistic, and account for the fact that the process becomes flatter for large t .

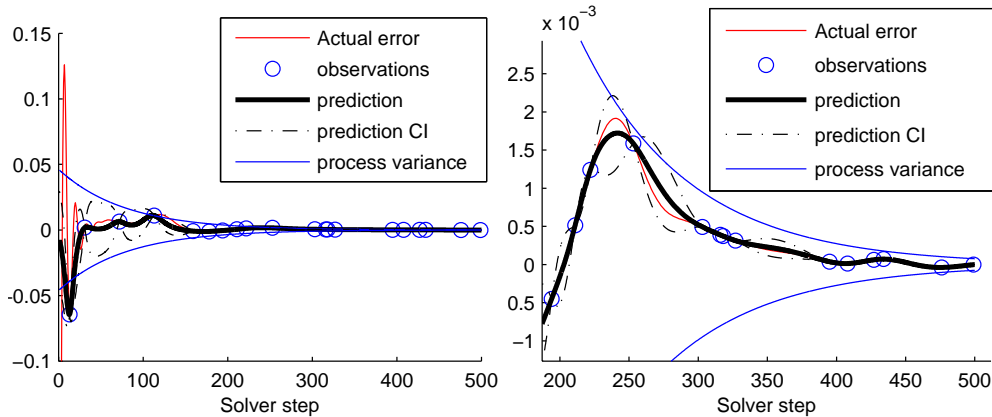


Figure 7: Example of error trajectory approximation using a GP model (left: complete trajectory, right: detail).

7.2 Learning design parameters

Now, for the remaining 182 designs of the learning DOE, partially converged simulations are run. 45 designs use the minimum convergence level (50 steps), another 45 use 60 steps, the other use random values between 50 and 500. With such setup, the DOE consists of four fully converged observations, one half of very inexpensive observations that ensures a good space filling, and the other half of heterogeneously converged observations. The total number of steps is equal to 18,500, which is the computational resource required to run 37 fully converged simulations.

The likelihood is maximized using the global optimizer CMA-ES [Hansen (2006)]. The estimated parameters are:

- $\hat{\sigma}_F^2 = 0.081$
- $\hat{\theta}_{Fx} = [2.00 \quad 0.98 \quad 1.38 \quad 1.48 \quad 0.51 \quad 2 \quad 1.22]$
- $\hat{\rho} = 0.523$ (meaning that F is smoother than G in the x direction)

7.3 7D analysis and comparison to Ordinary Kriging

Here, we compare our model to two versions of Ordinary Kriging:

- Ordinary (interpolating) Kriging based on 37 fully converged simulations,
- Ordinary (regressing) Kriging based on the 186 partially converged simulations

The first model corresponds to the standard situation (full convergence, interpolating model) and the number of observations is chosen so that the computational budget (i.e. total number of solver iterations) is equal to the budget of the partially converged DOE. The 37 points are chosen as a subset of the initial LHS using a maximin criterion to ensure a good space-filling. The second model is also standard and corresponds to a simplified error model: all the errors are treated as Gaussian, centered and independent of each other, with equal variances.

For both models, the parameters $\hat{\sigma}_F^2$ and $\hat{\theta}_{Fx}$ of the space-time model are used for the covariance. In addition for the regressing model, the diagonal matrix that accounts for the error variances is taken as $\Delta = \text{diag}([\sigma_G^2(t_1, t_1), \dots, \sigma_G^2(t_n, t_n)])$, which are the variances given by the space-time model. Hence, the differences between the three models are only due to the model structures and the design of experiments. In particular, this allows us to measure by how much we gain in prediction by using a complex error model. On both cases, it has been found that the space-time model parameters provide more accurate models than parameters estimated directly by maximum likelihood (in the case of the interpolating model, estimating the eight parameters of the anisotropic covariance based on 37 observations is nearly impossible); comparing these models is thus fair.

The predicting performances are given in Figure 8 and Table 3. The histograms represent the differences between the model means and the actual converged values, from which is also computed the RMSE (root mean square error) statistic. In addition, the 95% confidence intervals are drawn in order to visualize if the model uncertainty reflects the reality. To assess the global uncertainty of each model, the average prediction variance at test points (referred to as integrated mean square error [IMSE], which is the classical terminology in computer experiments [Sacks et al. (1989)]) and the maximum prediction variance (maxMSE) are computed.

For the space-time model, two actual values are outside the interval, which shows a relatively good calibration of the prediction variance. The OK with partially converged data is on the contrary over-confident, since almost half of the data is outside the interval. Inversely, the OK with fully converged data seems well calibrated (four data outside the intervals). The IMSE values confirm that the predicted uncertainty is a lot higher with 37 observations than with the space-time model.

The RMSE errors show that assuming that the errors are Gaussian, centered and independent of each other leads to a very poor model. The very high RMSE value is due to a strong bias in the model, in particular the high values of the actual function are most of the time underestimated (Figure 8, center). In comparison, using only fully converged simulations leads to a safer and more accurate model. The space-time model offers here the best results in terms of RMSE.

7.4 Optimal design of experiments for prediction

We have observed in the previous section that the average prediction variance was a lot smaller using partially converged simulations than using fully converged ones. In other words, the model was more accurate when spreading the budget into the 186 simulations instead of concentrating it on 37.

Table 3: Prediction statistics of the three models

<i>Model</i>	<i>RMSE</i>	<i>IMSE</i>	maxMSE
Space-Time	0.0542	0.0054	0.0163
Ordinary Kriging with 186 observations	0.1646	0.0061	0.0179
Ordinary Kriging with 37 observations	0.0755	0.0078	0.0286

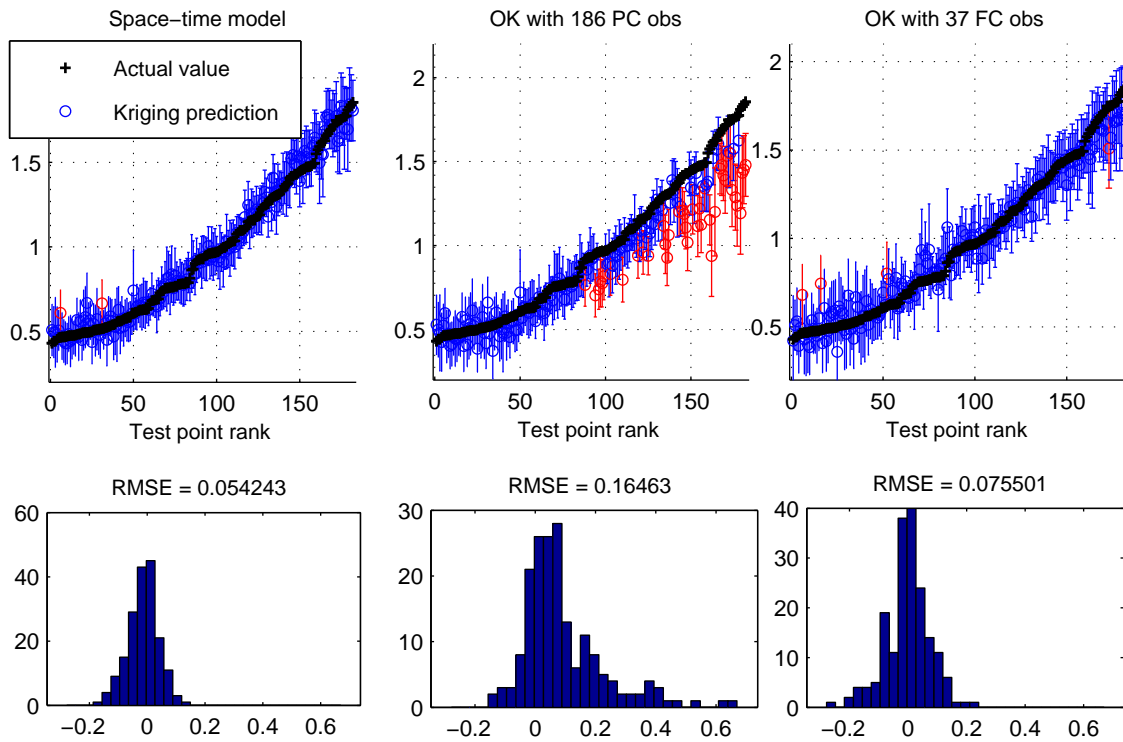


Figure 8: Comparison of the predicting capacity of the space-time model and two Ordinary Kriging models. The top figures show the actual responses values along with the predictions, represented by the mean (circle) and ± 1.96 times the standard deviation (errorbars). The 182 test points are ranked by their response value. Red errorbars indicate points where the actual value is outside the kriging 95% interval.

Finding the most efficient design of experiments for both learning parameters and prediction is already a challenging question with classical kriging models and seems an unreachable objective. However, it is possible to see if there exists an optimal trade-off between the number of observations and their precision, for a model with known parameters and given a fixed computational budget.

Here, we use the parameters values obtained previously, but we replace the existing DOE by a subset of the 186-point LHS with constant convergence level. The total budget is taken as 18,500, so the number of observations varies between 37 (with 500 steps for each simulation) and 186 (with 100 steps for each). The RMSE, IMSE and maxMSE metrics are computed in each case. Note that contrary to the RMSE, the IMSE and maxMSE do not depend on the observation values and can be computed off-line, so an optimal strategy for those criteria can be found before running any simulation (assuming that the parameters are known).

For each configuration, 20 subsets are taken randomly from the initial LHS. The results are presented in the form of boxplots in Figure 9.

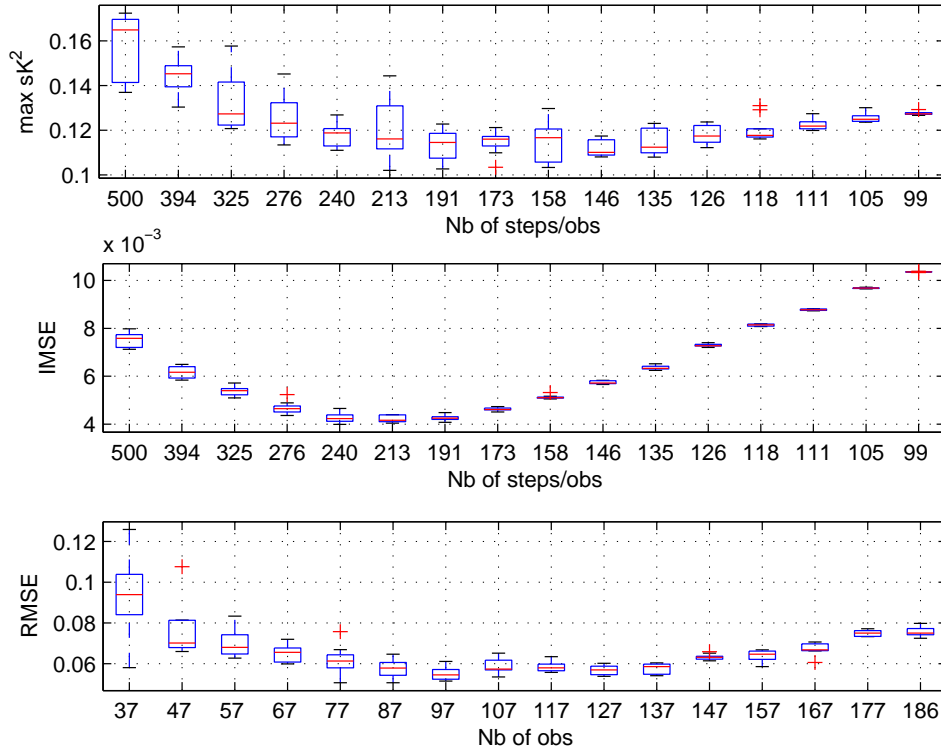


Figure 9: Boxplots of the RMSE, IMSE and maxMSE of the space-time model based on different DOE size for a constant computational budget of 18,500 steps. The abscissa is written either in terms of number of steps for one simulation or total number of simulations.

The boxplots clearly show that some sampling strategies are better than others. In terms of maximum prediction variance, using limited convergence and more simulations is more efficient, with optimal values for 146 steps (127 simulations). The maxMSE is very sensitive to holes in the design space, so using a large number of observations allows a better coverage of the design space. However, when the number of observations becomes to high (here 186), the response uncertainty overcomes this advantage.

Similarly, the IMSE shows that there is an optimal trade-off, here situated at 213 steps (87 observations). This trade-off is different from the one for the maxMSE criterion. For the error in the model mean, a trade-off again appears, but favors less accurate simulations. Here, no noticeable difference appears between 191 and 137 steps (97 and 137 observations, respectively). Note that these trade-offs may depend on the total

budget.

Here, using 97 observations with 191 steps for each seems a good trade-off between the three indicators. Such DOE, which has exactly the same budget as the one from §7, appears to be a lot better alternative with respect to maxMSE (0.11 instead of 0.16) and IMSE (0.0042 instead of 0.0054). Hence, learning with partial convergence may benefit very substantially from using optimal design strategies.

However, the difference between the IMSE and RMSE results indicate that theoretical criteria may not be the perfect, since they do not take into account any modeling error, which can be significant. Hence, a good alternative may be to choose a majority of simulations with optimal convergence level, and complete this design with a couple of simulations with heterogeneous convergence level in order to increase the robustness.

8 Conclusion

In this paper, we explored the possibility of using partially converged simulations for the approximation of expensive-to-evaluate computer codes. We have proposed to use Gaussian processes to approximate the simulator response in the joint design-time space. The main idea was to model the observed responses as a realization of a random process, which is the sum of a stationary process depending on design parameters only and of an error process which variance decreases towards zero when time tends to infinity. Appropriate covariance functions have been proposed to account for the decreasing variance and the additive structure. Then, the prediction equations (conditional on a set of observations) look like in the classical computer experiments framework.

When using such models, two major challenges arise: learning the model parameters and dealing with large data sets. We proposed solutions (decomposing the learning problem into a series of simpler optimization problems, and using screening effect) to account for both problems.

Finally, we have applied our model to the prediction of the output of a CFD simulator, and showed that using a space-time model provides a substantial improvement in accuracy compared to either using completely converged responses and an interpolating model, or using partially converged responses and a regressing model.

We believe that partial convergence can provide an efficient solution to alleviate the computational cost of many procedures involving computer experiments, and the proposed model may be used as a helping tool for uncertainty propagation, inverse problems, sensitivity analysis or optimization. Future research may include developments in this area.

References

- Alexandrov, N., R. Lewis, C. Gumbert, L. Green, and P. Newman (2000). Optimization with variable-fidelity models applied to wing design. *AIAA paper 841*(2000), 254.
- Cressie, N. (1993). *Statistics for Spatial Data, revised edition*, Volume 928. Wiley, New York.
- Dadone, A. and B. Grossman (2000). Progressive optimization of inverse fluid dynamic design problems. *Computers and Fluids* 29(1), 1–32.
- Dadone, A. and B. Grossman (2003). Fast convergence of inviscid fluid dynamic design problems. *Computers and Fluids* 32(4), 607–627.
- Forrester, A., N. Bressloff, and A. Keane (2006). Optimization using surrogate models and partially converged computational fluid dynamics simulations. *Proceedings of the Royal Society A* 462(2071), 2177.
- Forrester, A., A. Keane, and N. Bressloff (2006). Design and Analysis of “Noisy” Computer Experiments. *AIAA journal* 44(10), 2331.
- Forrester, A., A. Sóbester, and A. Keane (2007). Multi-fidelity optimization via surrogate modelling. *Proceedings of the Royal Society A: Mathematical, Physical and Engineering Science* 463(2088), 3251–3269.

- Gano, S., J. Renaud, J. Martin, and T. Simpson (2006). Update strategies for kriging models used in variable fidelity optimization. *Structural and Multidisciplinary Optimization* 32(4), 287–298.
- Gumbert, C., P. Newman, and G. Hou (2001). Simultaneous aerodynamic analysis and design optimization(saado) for a 3-d flexible wing. In *AIAA, Aerospace Sciences Meeting and Exhibit, 39 th, Reno, NV*.
- Han, Z., R. Zimmermann, and S. Görtz (2010). A new cokriging method for variable-fidelity surrogate modeling of aerodynamic data. In *48th AIAA Aerospace Sciences Meeting Including the New Horizons Forum and Aerospace Exposition, Orlando, FL*, pp. 2010–1225.
- Hansen, N. (2006). The cma evolution strategy: a comparing review. *Towards a new evolutionary computation*, 75–102.
- Huang, D., T. Allen, W. Notz, and R. Miller (2006). Sequential kriging optimization using multiple-fidelity evaluations. *Structural and Multidisciplinary Optimization* 32(5), 369–382.
- Jones, D., M. Schonlau, and W. Welch (1998). Efficient global optimization of expensive black-box functions. *Journal of Global Optimization* 13(4), 455–492.
- Kennedy, M. and A. O’Hagan (2000). Predicting the output from a complex computer code when fast approximations are available. *Biometrika* 87(1), 1.
- Kyriakidis, P. and A. Journel (1999). Geostatistical space–time models: a review. *Mathematical geology* 31(6), 651–684.
- Laurenceau, J. and P. Sagaut (2008). Building efficient response surfaces of aerodynamic functions with kriging and cokriging. *AIAA journal* 46(2), 498.
- Lewis, R. and S. Nash (2005). Model problems for the multigrid optimization of systems governed by differential equations. *SIAM Journal on Scientific Computing* 26(6), 1811–1837.
- Matheron, G. (1969). Le krigeage universel. *Cahiers du centre de morphologie mathématique* 1.
- Qian, P. and C. Wu (2008). Bayesian hierarchical modeling for integrating low-accuracy and high-accuracy experiments. *Technometrics* 50(2), 192–204.
- Rasmussen, C. and C. Williams (2006). *Gaussian processes for machine learning*. Springer.
- Roustant, O., D. Ginsbourger, and Y. Deville (2012). DiceKriging, DiceOptim: Two R Packages for the Analysis of Computer Experiments by Kriging-Based Metamodeling and Optimization. *Journal of Statistical Software* 51 (1), 1–55.
- Sacks, J., W. Welch, T. Mitchell, and H. Wynn (1989). Design and analysis of computer experiments. *Statistical science*, 409–423.
- Santner, T., B. Williams, and W. Notz (2003). *The Design and Analysis of Computer Experiments*. Springer.
- Stein, M. (1999). *Interpolation of spatial data: some theory for kriging*. Springer Verlag.
- Stein, M. (2002). The screening effect in kriging. *Annals of statistics*, 298–323.
- Yamazaki, W. and D. Mavriplis (2011). Derivative-Enhanced Variable Fidelity Surrogate Modeling for Aerodynamic Functions. In *AIAA, Aerospace Sciences Meeting and Exhibit, 49 th, Orlando FL, January 4-7*.

Appendix: screening effect in the time dimension in the case of Monte-Carlo convergence

Property: Once the \tilde{Y}_i are taken into account in the model, adding any $Y(\mathbf{u})$ with $\mathbf{u} = (\mathbf{x}^i, t_u)$ for $i \in \{1, \dots, n\}$ and $t_u \leq t_i$ has no effect on the model.

Proof:

Let us denote by $\lambda_1, \dots, \lambda_n$ the kriging weights corresponding to a prediction at an arbitrary point $\mathbf{x} \in D$ when $\tilde{Y}_1, \dots, \tilde{Y}_n$ are known, the kriging mean being equal to $\sum_{k=1}^n \lambda_k \tilde{Y}_k$. By characterization of the kriging mean as projection of $Y(\mathbf{x})$ onto $\text{Span}\{\tilde{Y}_1, \dots, \tilde{Y}_n\}$, we know that:

$$E \left[\left(Y(\mathbf{x}) - \sum_{k=1}^n \lambda_k \tilde{Y}_k \right) \tilde{Y}_i \right] = 0, \quad \forall i \in \{1, \dots, n\} \quad (31)$$

We will now show that $Y(\mathbf{x}) - \sum_{k=1}^n \lambda_k \tilde{Y}_k$ is also orthogonal to $Y(\mathbf{u})$, which is a sufficient condition for the conditional independence in question.

Indeed, denoting S the scalar product between those two quantities, we have:

$$S = E \left[\left(Y(\mathbf{x}) - \sum_{k=1}^n \lambda_k \tilde{Y}_k \right) \tilde{Y}(\mathbf{u}) \right] \quad (32)$$

$$= E \left[\left(Y(\mathbf{x}) - \sum_{k=1}^n \lambda_k \tilde{Y}_k \right) \left(F(x^i) + \frac{1}{t_u} \sum_{j=1}^{t_u} \varepsilon_{i,j} \right) \right] \quad (33)$$

$$= E \left[\left(Y(\mathbf{x}) - \sum_{k=1}^n \lambda_k \tilde{Y}_k \right) \left(\tilde{Y}_i - \frac{1}{t_i} \sum_{j=1}^{t_i} \varepsilon_{i,j} + \frac{1}{t_u} \sum_{j=1}^{t_u} \varepsilon_{i,j} \right) \right] \quad (34)$$

$$= E \left[\left(Y(\mathbf{x}) - \sum_{k=1}^n \lambda_k \tilde{Y}_k \right) \left(\frac{1}{t_u} \sum_{j=1}^{t_u} \varepsilon_{i,j} - \frac{1}{t_i} \sum_{j=1}^{t_i} \varepsilon_{i,j} \right) \right], \quad (35)$$

\tilde{Y}_i being removed due to eq. 31.

Then, hypothesizing all the $\varepsilon_{i,j}$ are independent of each other and have an expectation equal to zero yields a null expectation for the term on the right parenthesis. Since $Y(\mathbf{x})$ and $\lambda_k \tilde{Y}_k$ are independent of $\varepsilon_{i,j}$ for $k \neq i$, eq. 35 reduces to:

$$S = E \left[-\lambda_i \tilde{Y}_i \left(\frac{1}{t_u} \sum_{i=1}^{t_u} \varepsilon_{i,j} - \frac{1}{t_i} \sum_{i=1}^{t_i} \varepsilon_{i,j} \right) \right] \quad (36)$$

Then:

$$S = E \left[-\lambda_i \left(F(\mathbf{x}^i) + \frac{1}{t_i} \sum_{j=1}^{t_i} \varepsilon_{i,j} \right) \left(\frac{1}{t_u} \sum_{j=1}^{t_u} \varepsilon_{i,j} - \frac{1}{t_i} \sum_{i=1}^{t_i} \varepsilon_{i,j} \right) \right] \quad (37)$$

$$= -\lambda_i E \left[\left(\frac{1}{t_i} \sum_{j=1}^{t_i} \varepsilon_{i,j} \right) \left(\frac{1}{t_u} \sum_{j=1}^{t_u} \varepsilon_{i,j} - \frac{1}{t_i} \sum_{j=1}^{t_i} \varepsilon_{i,j} \right) \right] \quad (38)$$

$$= -\lambda_i \left(\frac{1}{t_u t_i} \sum_{j=1}^{t_u} \sum_{k=1}^{t_i} E[\varepsilon_{i,j} \varepsilon_{i,k}] - \frac{1}{t_i^2} \sum_{j=1}^{t_u} \sum_{k=1}^{t_i} E[\varepsilon_{i,j} \varepsilon_{i,k}] \right) \quad (39)$$

$$= -\lambda_i \left(\frac{1}{t_u t_i} \sum_{j=1}^{t_u} \sum_{k=1}^{t_i} \delta_{j,k} - \frac{1}{t_i^2} \sum_{j=1}^{t_u} \sum_{k=1}^{t_i} \delta_{j,k} \right) \quad (40)$$

$$= -\lambda_i \left(\frac{1}{t_u t_i} t_u - \frac{1}{t_i^2} t_i \right) \quad (41)$$

$$= 0 \quad (42)$$